

# Siege of the South: Hunga Tonga-Hunga Ha'apai Water Vapor Excluded from 2022 Antarctic Stratospheric Polar Vortex

Gloria L. Manney<sup>1,2</sup>, Michelle L. Santee<sup>3</sup>, Alyn Lambert<sup>3</sup>, Luis F. Millán<sup>3</sup>, Ken Minschwaner<sup>2</sup>, Frank Werner<sup>3</sup>, Zachary D. Lawrence<sup>4,5</sup>, William G. Read<sup>3</sup>, Nathaniel J. Livesey<sup>3</sup>, Tao Wang<sup>3</sup>

<sup>1</sup>NorthWest Research Associates, Socorro, NM, USA

<sup>2</sup>New Mexico Institute of Mining and Technology, Socorro, NM, USA

<sup>3</sup>Jet Propulsion Laboratory, California Institute of Technology, Pasadena, CA, USA

<sup>4</sup>Cooperative Institute for Research in Environmental Sciences (CIRES) & NOAA Physical Sciences Laboratory (PSL),

University of Colorado, Boulder, Colorado, USA.

<sup>5</sup>NorthWest Research Associates, Boulder, CO, USA

## Key Points:

- MLS trace gas data show that the Hunga Tonga-Hunga Ha'apai H<sub>2</sub>O plume was effectively excluded from the 2022 Antarctic polar vortex
- Antarctic lower stratospheric vortex strength, size, and longevity were among the largest on record, but within the range of previous years
- Antarctic chemical ozone loss in 2022 was unexceptional, with MLS ozone and related trace gases observed to be near average

---

Corresponding author: Gloria L Manney, [manney@nwra.com](mailto:manney@nwra.com)

## Abstract

We use Aura Microwave Limb Sounder (MLS) trace gas measurements to investigate whether water vapor ( $\text{H}_2\text{O}$ ) injected into the stratosphere by the Hunga Tonga-Hunga Ha'apai (HTHH) eruption affected the 2022 Antarctic stratospheric vortex. Other MLS-measured long-lived species are used to distinguish high HTHH  $\text{H}_2\text{O}$  from that descending in the vortex from the upper-stratospheric  $\text{H}_2\text{O}$  peak. HTHH  $\text{H}_2\text{O}$  reached high southern latitudes in June–July but was effectively excluded from the vortex by the strong transport barrier at its edge. MLS  $\text{H}_2\text{O}$ , nitric acid, chlorine species, and ozone within the 2022 Antarctic polar vortex were near average; the vortex was large, strong, and long-lived, but not exceptionally so. There is thus no clear evidence of HTHH influence on the 2022 Antarctic vortex or its composition. Substantial impacts on the stratospheric polar vortices are expected in succeeding years since the  $\text{H}_2\text{O}$  injected by HTHH has spread globally.

## Plain Language Summary

The 2022 Hunga Tonga-Hunga Ha'apai eruption injected vast amounts of water vapor into the stratosphere. There has been much speculation that this large increase in water vapor could impact the Antarctic stratospheric polar vortex and Antarctic ozone hole: Water vapor plays an important role in polar vortex ozone depletion by providing the necessary conditions for the formation of polar stratospheric clouds. These clouds provide surfaces on which ozone-depleting chemical reactions can occur. The excess water vapor could also change the vortex evolution via water vapor's effects on temperature, which could in turn affect the strong band of winds demarcating the polar vortex edge. We use satellite measurements of water vapor and other gasses to show that by the time the water vapor from the Hunga Tonga volcanic eruption reached the south polar regions in June–July 2022, the polar vortex was too strong for it to penetrate. Measurements of water vapor, ozone, and chemicals involved in destroying ozone all showed near-average amounts and evolution within the vortex. In future years, larger effects on the polar vortex and chemical processing are expected because water vapor from Hunga Tonga that has spread globally will be entrained into the polar vortex.

## 1 Introduction

The 15 January 2022 eruption of the underwater volcano Hunga Tonga-Hunga Ha'apai (HTHH) injected an unprecedented amount of water vapor ( $\text{H}_2\text{O}$ ) directly into the stratosphere, increasing the stratospheric  $\text{H}_2\text{O}$  burden by approximately 10% (e.g., Millán et al., 2022; Vömel et al., 2022). It also resulted in substantial, though not unprecedented, enhancements in volcanic aerosol loading (Khaykin et al., 2022; Sellitto et al., 2022; Taha et al., 2022). Numerous studies have already explored aspects of the stratospheric impacts of HTHH enhancements in aerosol and  $\text{H}_2\text{O}$ ; of particular relevance here are suggestions that  $\text{H}_2\text{O}$  and aerosol from HTHH injected into the Southern Hemisphere (SH) stratosphere took many months to reach high latitudes and did not extend poleward of about  $60^\circ\text{S}$  (e.g., Legras et al., 2022; Khaykin et al., 2022; Schoeberl et al., 2022; Zhu et al., 2022). In the lowermost stratosphere (at and below approximately the 380 K isentropic surface), a few studies suggest that some  $\text{H}_2\text{O}$  and aerosol were transported to high SH latitudes within days to weeks via the shallow branch of the Brewer-Dobson circulation (e.g. Taha et al., 2022; Schoeberl et al., 2022; Khaykin et al., 2022). Radiative cooling from HTHH  $\text{H}_2\text{O}$  led to unprecedented cold in SH mid/low latitudes, with associated circulation and transport anomalies (Coy et al., 2022; Schoeberl et al., 2022; Sellitto et al., 2022).

It was suggested that transport of HTHH aerosol and  $\text{H}_2\text{O}$  into high SH latitudes might impact the composition of the 2022 SH stratospheric polar vortex, and that circulation changes associated with the HTHH  $\text{H}_2\text{O}$  plume might affect the strength, size, and / or longevity of that vortex (e.g., Taha et al., 2022; Zhu et al., 2022). Here we use Aura Microwave Limb Sounder (MLS) data to analyze the evolution of the SH stratospheric polar vortex in 2022, transport of the HTHH  $\text{H}_2\text{O}$  plume in relation to it, and chemical processing within it. We find no evidence of substantial impacts of HTHH on the 2022 SH polar vortex or the chemical processing and ozone loss within it. We use temperature,  $\text{H}_2\text{O}$ ,  $\text{N}_2\text{O}$ , CO, HCl, ClO, and  $\text{O}_3$  from v5 MLS “level 3” (L3)

69 data (Livesey et al., 2020), along with meteorological fields from NASA’s Modern Era Retrospective-  
 70 analysis for Research and Applications Version 2 (MERRA-2) dataset (Gelaro et al., 2017; Global  
 71 Modeling and Assimilation Office (GMAO), 2015).

72 Immediately following the eruption, standard MLS v5 quality screening (Livesey et al., 2020)  
 73 flagged many of the profiles most affected by HTHH as suspect retrievals (Millán et al., 2022);  
 74 thus the H<sub>2</sub>O, N<sub>2</sub>O, and HNO<sub>3</sub> anomalies shown here may be artificially small for up to three  
 75 weeks after the eruption. Since our focus is on the subsequent transport and relationship to the  
 76 SH polar vortex, our results are unaffected.

## 77 2 Transport of HTHH Stratospheric H<sub>2</sub>O

78 Figure 1 shows the evolution of N<sub>2</sub>O and H<sub>2</sub>O (both generally long-lived tracers of trans-  
 79 port in the stratosphere) anomalies in the SH lower through middle stratosphere, in vortex av-  
 80 erages as a function of height (expressed as potential temperature,  $\theta$ ) and as a function of equiv-  
 81 alent latitude (EqL, the latitude enclosing the same area between it and the pole as a given po-  
 82 tential vorticity, PV, contour, Butchart & Remsberg, 1986) on several isentropic ( $\theta$ ) surfaces. The  
 83 past five years include seasons with exceptionally warm / short-lived (2019) and cold / long-lived  
 84 (2020 and 2021) springtime polar vortices, as well as a year (2018) with more typical vortex char-  
 85 acteristics (WMO, 2023). (Figs. S1–S2 in the Supporting Information, SI, show the full-mission  
 86 and include MLS temperature.) The evolution of vortex-average N<sub>2</sub>O (Fig. 1a) in 2022 is unex-  
 87 ceptional, showing positive anomalies except at the lowest levels; such a vertical dipole pattern  
 88 of N<sub>2</sub>O anomalies is common, with primarily higher values in 2020, 2021, and 2022 consistent  
 89 with lower vortex temperatures (see below and Figs. S1–3) and accompanying weaker diabatic  
 90 descent (Fig. S4). N<sub>2</sub>O EqL/time evolution (Fig. 1b–f) is also fairly typical; recurring changes  
 91 above 430 K from high to low anomalies extending from low latitudes show quasi-biennial os-  
 92 cillation (QBO) related transport (e.g., Baldwin et al., 2001; Diallo et al., 2019). Low N<sub>2</sub>O anoma-  
 93 lies in austral spring 2020 and 2021 are related to the delayed vortex breakup in those years, with  
 94 low N<sub>2</sub>O values remaining confined longer in a more persistent vortex. Spring 2022 shows simi-  
 95 lar, but weaker, anomalies, suggesting a long-lived vortex. In contrast, high anomalies in 2019  
 96 result from a rare SH sudden stratospheric warming that led to a small, warm, and short-lived vor-  
 97 tex (e.g., Wargan et al., 2020).

98 H<sub>2</sub>O anomalies (Fig. 1g–l) in the SH lower stratospheric vortex are typically dominated  
 99 by interannual variations in polar stratospheric cloud extent; strong low H<sub>2</sub>O anomalies in spring  
 100 2020 and 2021 at 500 K and surrounding levels arose from persistent cold anomalies in unusu-  
 101 ally long-lasting vortices. Outside the vortex (Fig. 1h–l), high H<sub>2</sub>O anomalies often ac-  
 102 company low N<sub>2</sub>O anomalies because H<sub>2</sub>O and N<sub>2</sub>O have opposite vertical and horizontal gra-  
 103 dients in the lower to middle stratosphere. For example, low (high) springtime H<sub>2</sub>O (N<sub>2</sub>O) anoma-  
 104 lies just outside the vortex edge in 2019, and opposite patterns in 2020 and 2021 at 600–850 K;  
 105 similar patterns are seen in mid-Eqls in earlier years (Fig. S1). (Note that typical H<sub>2</sub>O anoma-  
 106 lies prior to 2022 are washed out by the large colorbar range needed to portray the HTHH H<sub>2</sub>O.)  
 107 Above 500 K, typical signatures of extra-vortex transport of H<sub>2</sub>O are overwhelmed by the arrival  
 108 of HTHH H<sub>2</sub>O (Fig. 1h–j, Fig. S1). HTHH H<sub>2</sub>O reached the vortex edge in early June 2022, af-  
 109 ter the vortex was fully developed except in the lowermost stratosphere. Above 500 K, extremely  
 110 strong gradients along the vortex edge suggest that the HTHH plume could not penetrate the vor-  
 111 tex edge. Pervasive high H<sub>2</sub>O anomalies since early 2020 below about 500 K may reflect linger-  
 112 ing enhancements from the 2020 Australian New Years fires (e.g., Santee et al., 2022). While small  
 113 positive anomalies encroach into the vortex region in late winter 2022 at 500 K (near the low-  
 114 est altitude of large HTHH enhancement) and 430 K, similar features are common (e.g., in 2018  
 115 and 2021), so it is unclear whether they are related to the HTHH plume. At all levels examined  
 116 (including the lowermost stratosphere, e.g., Fig. S3), H<sub>2</sub>O anomalies inside the vortex are within  
 117 the typical range.

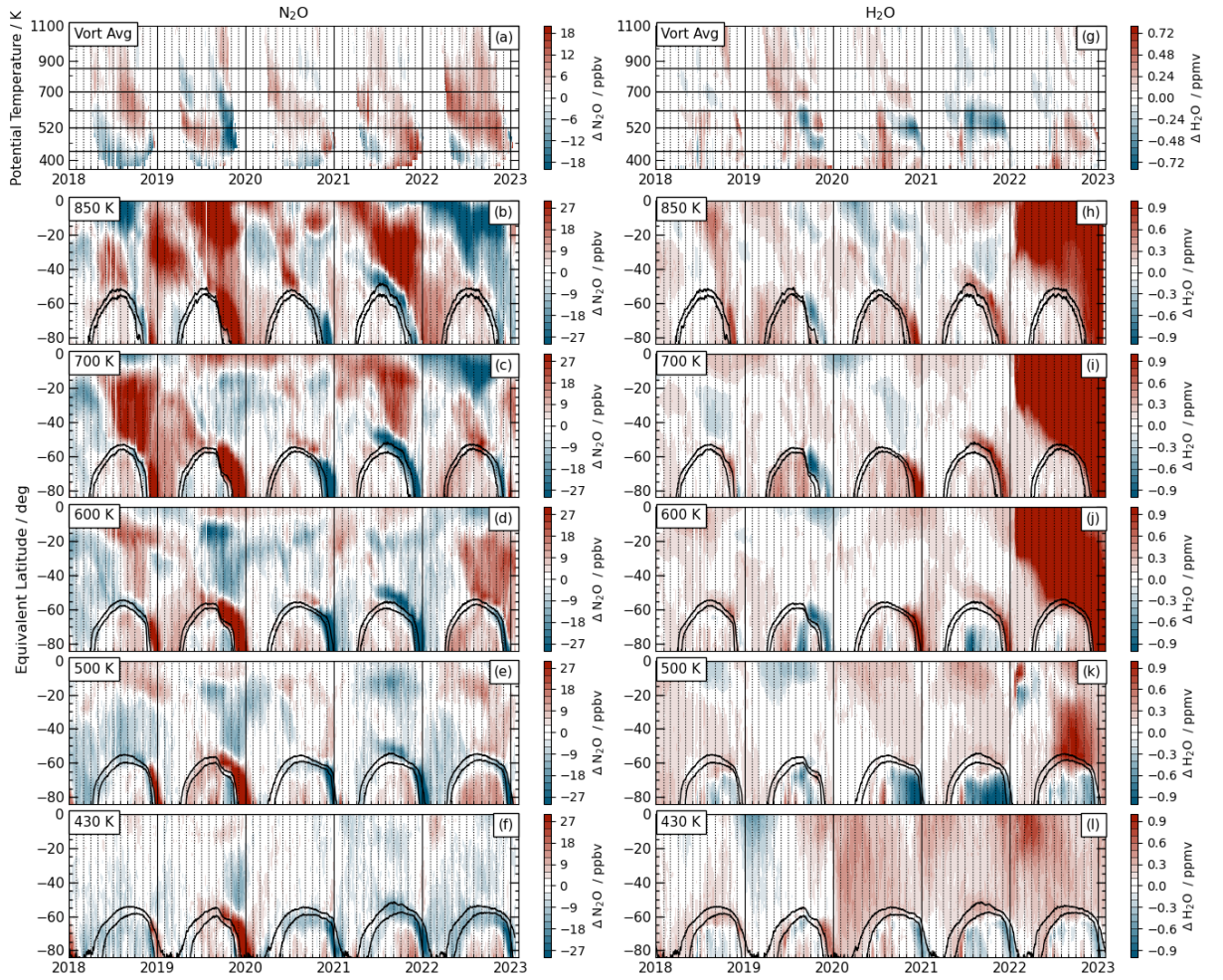


**Figure 1.** Evolution of MLS-observed SH anomalies from the baseline 2005–2021 climatology of  $\text{N}_2\text{O}$  (a–f) and  $\text{H}_2\text{O}$  (g–l) from January 2018 through January 2023: (a,g) vortex-averaged values; (b–f, h–l) evolution as a function of EqL at levels in the middle through lower stratosphere (horizontal lines in a,g). Black contours in b–f and h–l are sPV values indicating the vortex edge region.

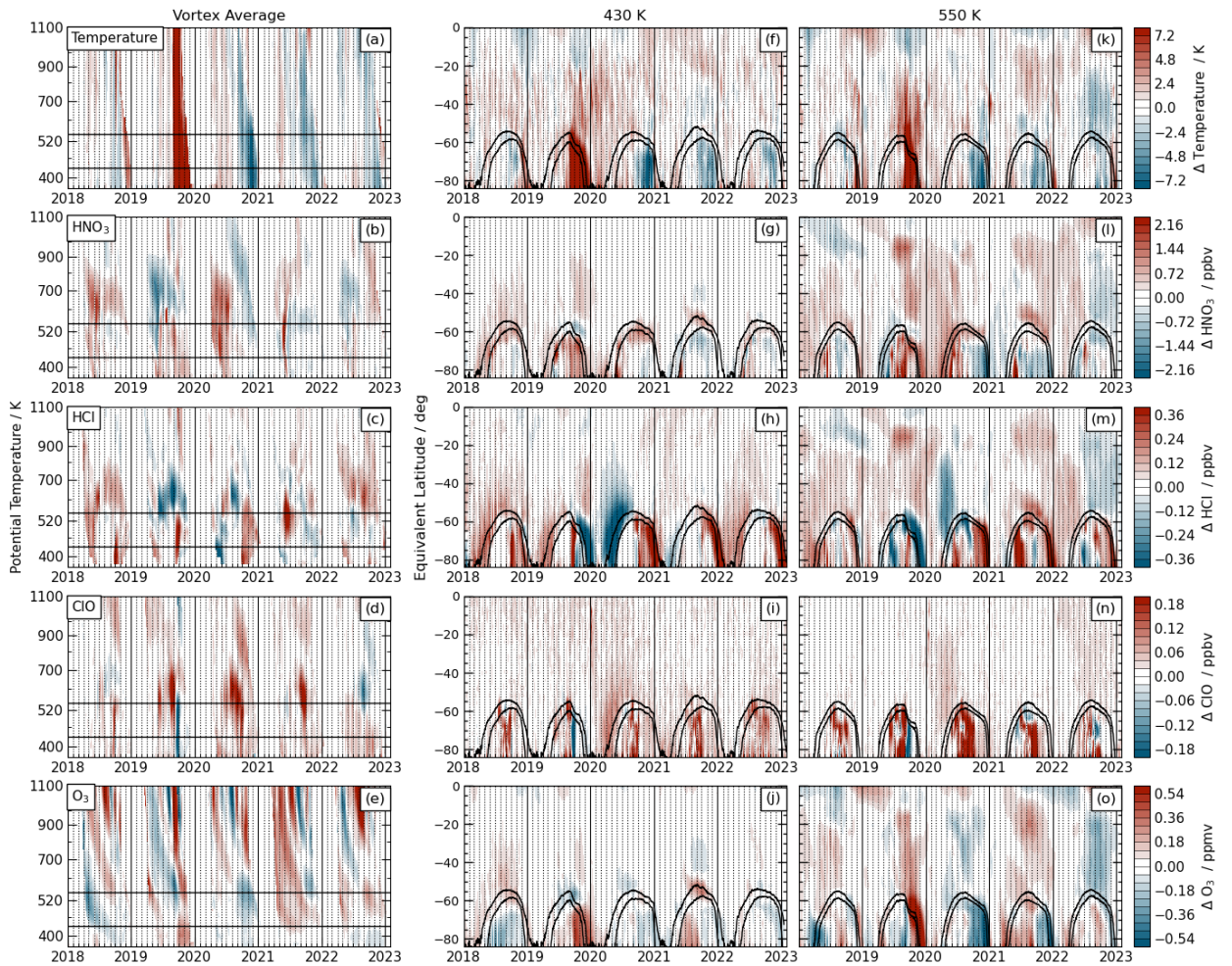


**Figure 2.** As in Fig. 1, but for MLS temperature,  $\text{HNO}_3$ ,  $\text{HCl}$ ,  $\text{ClO}$ , and  $\text{O}_3$ ; (a–e) vortex averages, (f–j) 430 K, and (k–o) 550 K EqL timeseries, for January 2018 through January 2023. Black contours (f–o) are sPV values demarking the vortex edge region.

118

### 3 Polar Vortex Composition and Chemical Processing

119

120

121

122

123

124

125

126

127

128

129

130

131

132

Figure 2 shows a similar view of MLS measurements of temperature and species involved in polar chemical processing (Figs. S1–3 show 550 K, 430 K, and 380 K for the full mission). The Antarctic vortex was unusually cold and persistent in spring 2022, but less so than in 2020 and 2021. Vortex  $\text{HNO}_3$  values were near average throughout the season. Vortex  $\text{HCl}$  and  $\text{ClO}$  commonly oscillate between high and low anomalies, and thus they are also generally unexceptional within the 2022 vortex; the high  $\text{HCl}$  anomalies in spring are related primarily to longer-than-usual confinement of the very high values that ensue from chlorine deactivation. Consistent with near-average vortex values of chlorine species,  $\text{O}_3$  anomalies in 2022 were also relatively small. Both 2020 and 2021 showed lower  $\text{O}_3$ , consistent with larger cold anomalies and even longer-lived (see below) vortices in those years than in 2022. Outside the vortex, temperature anomalies (arising from radiative effects of HTHH  $\text{H}_2\text{O}$ , e.g., Coy et al., 2022; Schoeberl et al., 2022) and associated mid-latitude transport anomalies (Coy et al., 2022) appear consistent with the extravortex high  $\text{N}_2\text{O}$  anomalies seen near 500–600 K (Fig. 1), and suggest that accompanying extravortex  $\text{HCl}$ ,  $\text{HNO}_3$ , and  $\text{O}_3$  anomalies are at least partially transport-driven.

Figure 3 provides a closer look at the  $E_{qL}/\theta$  evolution of MLS trace gases in 2022, showing snapshots of anomalies from climatology (similar anomaly plots in 2018, 2020, and 2021 are shown in Figs. S5–S7). The  $H_2O$  plume first approached the SH polar vortex edge in early to mid-June. Subsequently, extremely strong  $H_2O$  gradients developed along the vortex edge over 520–800 K and persisted through October (into December below about 700 K; see also Fig 1). By mid-December, only a weak remnant of the vortex remained below about 520 K, and the  $H_2O$  enhancement extended into high latitudes above that level. MLS data show no indication of air from the HTHH  $H_2O$  plume penetrating substantially into the SH vortex before its breakup.  $N_2O$  anomalies within the vortex were generally small until austral spring; below about 700 K, these anomalies were near zero from August through October. Low  $N_2O$  anomalies along the vortex edge beginning in early November are consistent with confinement in an unusually persistent vortex. Mid-latitude cold anomalies throughout the middle stratosphere (e.g., Coy et al., 2022; Schoeberl et al., 2022) are apparent from June through mid-December. Vortex temperatures were below average through much of the season, with largest cold anomalies in October and November (also see Fig. 2). High extra-vortex  $N_2O$  anomalies through this period are consistent in extent and location with the circulation anomalies reported by Coy et al. (2022). The co-location of  $N_2O$  anomalies with those in  $HNO_3$ , HCl, and  $O_3$  suggests that transport plays a role in all of them; work is in progress analyzing the relative effects of dynamical and chemical processes.

Within the vortex,  $HNO_3$  is slightly lower than usual, consistent with a colder-than-average vortex. HCl (ClO) shows low (high) anomalies during much (but not all, e.g., Fig. 3A,G) of the winter. As noted above, high HCl anomalies appear along the vortex edge in November and in the vortex remnant in mid-December, consistent with high values resulting from deactivation into HCl (as is typical in the SH, e.g., Santee et al., 2008) followed by unusually enduring confinement in the persistent vortex. Lower stratospheric  $O_3$  anomalies in the early winter (before extensive chemical loss) are slightly positive and remain so through October (e.g., Fig. 3O). Taken together, the results in Figs. 2 and 3 suggest that the modest low anomalies in  $O_3$  seen in austral spring 2022 (e.g., Fig. 3P) result primarily (if not entirely) from the unusual persistence of the vortex.

#### 4 Vortex Evolution and Trace Gas Confinement

Figure 4 summarizes the evolution of the 2022 SH vortex in the context of the 43-year MERRA-2 record and the evolution of trace gases in the context of the 18-year MLS record, both in relation to the previous three SH winters. Figure S8 shows profiles of additional MERRA-2 diagnostics of vortex strength and longevity. Consistent with the indications in the trace gases of its unusual persistence, the 2022 SH late winter and spring vortex was among the largest on record at levels up to about 650 K, approximately matching the maximum size and persistence seen prior to 2020 (Fig. 4a–d; Fig. S8b,d). In spring, the 2021 vortex area was slightly larger, and the 2020 vortex area substantially larger than that in 2022 from about 460 K to 650 K, with 2020 setting the record for lower-stratospheric vortex persistence (Fig. 4a–c, S8b–d). Maximum PV gradients, indicating vortex strength (that is, robustness as a transport barrier), show unusually strong springtime vortices in 2020 through 2022 below about 500 K, but only the 2020 vortex was stronger than average above about 600 K (Fig. 4e–h; Fig. S8a). Below about 520 K, the area with temperatures below the nitric acid trihydrate (NAT) and ice polar stratospheric cloud (PSC) thresholds was larger than usual (Fig 4m,n,q,r) and PSCs persisted later than usual (Fig. 4m–t, Fig. S8e,f) in spring 2020, 2021, and 2022, but only exceeded previous springtime records in 2020; above about 600 K PSC area and duration were near average.

The unexceptional MLS trace gas evolution in the 2022 Antarctic vortex is highlighted in Fig. 4A–P (Fig. S9 shows the vertical structure). Interannual variability in SH polar chemical processing is relatively small, but, with few exceptions, all of the trace gases show 2022 evolution that is well within the previously observed range. Over  $\sim 450$ –600 K, persistently low  $H_2O$  after October in 2022, and to an even greater extent in 2020 and 2021, is consistent with confinement of dehydrated air in long-lived vortices. Chlorine evolution (seen in HCl and ClO, Fig. 4E–

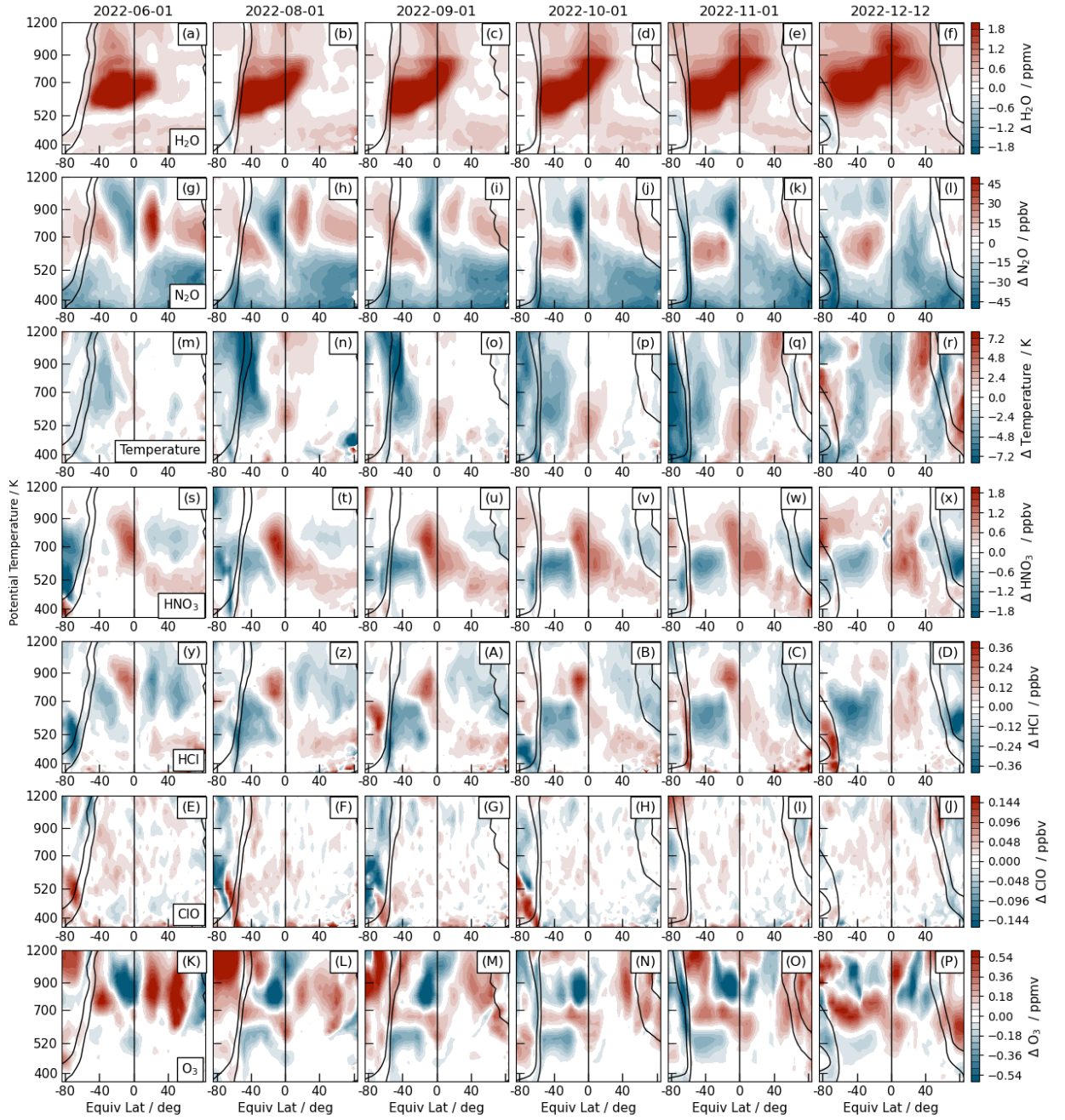


**Figure 3.** Snapshots on selected days in 2022 of anomalies from the baseline 2005–2021 climatology of MLS (a–f)  $\text{H}_2\text{O}$ , (g–l)  $\text{N}_2\text{O}$ , (m–r) temperature, (s–x)  $\text{HNO}_3$ , (y–D)  $\text{HCl}$ , (E–J)  $\text{ClO}$ , and (K–P)  $\text{O}_3$ . Black contours show sPV values demarking the vortex edge region.

184 L; Fig. S9q–x) was fairly typical throughout the season. Observed O<sub>3</sub> evolution in 2022 was re-  
 185 markably near average throughout the season (Fig. 4M–P; Fig. S9y–B).

186 The above results provide visual evidence that the vortex edge presented an effective trans-  
 187 port barrier, preventing substantial penetration of the HTHH H<sub>2</sub>O plume. To look more closely  
 188 at the robustness of the vortex edge transport barrier, Fig. 5 shows scatter and density plots of H<sub>2</sub>O  
 189 versus N<sub>2</sub>O and sPV for representative days in 2022 compared with the evolution in all prior years  
 190 in the MLS record. Low N<sub>2</sub>O (relative to the range of values at a given level) and high-magnitude  
 191 sPV identify vortex air parcels. In the lower stratosphere (exemplified by 550 K), increasingly  
 192 low vortex H<sub>2</sub>O through the season results from dehydration and is very similar to that previously  
 193 observed by MLS (density plots, right columns, emphasize the similarity of the main distribu-  
 194 tions in 2022 to those in earlier years). Extravortex H<sub>2</sub>O at 550 K does not stand out from the pre-  
 195 vious record before July, but after that the HTHH enhancement manifests as a distinct cluster of  
 196 high H<sub>2</sub>O with N<sub>2</sub>O near 200 ppbv and sPV magnitudes  $< 1 \times 10^{-4} \text{ s}^{-1}$  (both values that are un-  
 197 ambiguously extravortex) that is unique to 2022 (compare yellow-orange / purple H<sub>2</sub>O / sPV val-  
 198 ues with grey dots; orange with grey contours). In the middle stratosphere (exemplified by 700 K),  
 199 vortex H<sub>2</sub>O values first increase via descent of the upper stratospheric peak, then decrease as con-  
 200 tinuing descent brings low mesospheric H<sub>2</sub>O into the stratospheric vortex (e.g., Ray et al., 2002;  
 201 Lee et al., 2011); both the high (e.g., Fig. 5a–d) and the low (e.g., Fig. 5e–l) H<sub>2</sub>O values that de-  
 202 scend through the vortex (low N<sub>2</sub>O, high-magnitude sPV end of the x-axis) at 700 K are distinct  
 203 from the extravortex population of high H<sub>2</sub>O from HTHH, and that is in turn distinguished from  
 204 extravortex air in previous years by higher H<sub>2</sub>O values at extravortex N<sub>2</sub>O (~150–200 ppbv) and  
 205 sPV (magnitude  $< \sim 1 \times 10^{-4} \text{ s}^{-1}$ ). These correlations of H<sub>2</sub>O with N<sub>2</sub>O and sPV (especially the  
 206 density plots versus sPV) show clearly that the air with enhanced H<sub>2</sub>O from HTHH remained well  
 207 separated from that within the vortex until vortex breakup at each level (as suggested in Figs. 1  
 208 and 3). MLS H<sub>2</sub>O / CO correlations show a similar picture in the middle (Fig. S10) and upper  
 209 stratosphere, with HTHH H<sub>2</sub>O associated with low CO values characteristic of extravortex air.  
 210 Further, because the seawater from HTHH has a higher ratio of HDO to H<sub>2</sub>O than background  
 211 water vapor in the extravortex stratosphere (e.g., Randel et al., 2012; Khaykin et al., 2022), an  
 212 unprecedented increase in that ratio in SH midlatitudes also marks the HTHH air as separate from  
 213 (and excluded from) that in the vortex (Figs. S11–12).

## 214 5 Summary

215 The unprecedented water vapor injection into the stratosphere by HTHH is tracked using  
 216 MLS and reanalysis data. The H<sub>2</sub>O plume [or The enhanced H<sub>2</sub>O] is shown to have been ef-  
 217 fectively excluded from the 2022 Antarctic polar vortex until the vortex breakdown. In contrast  
 218 to speculation that HTHH stratospheric H<sub>2</sub>O and aerosol injections would lead to substantial anoma-  
 219 lies in the Antarctic polar vortex and lower stratospheric polar processing and ozone loss within  
 220 it (e.g., Taha et al., 2022; Zhu et al., 2022), our analysis suggests that HTHH did not cause sub-  
 221 stantial changes in polar processing and ozone loss within the vortex: MLS observations of HNO<sub>3</sub>,  
 222 HCl, ClO, and O<sub>3</sub> inside the vortex through the depth of the lower stratosphere all show evolu-  
 223 tion well within the range of previous years during the MLS mission, with near-average O<sub>3</sub> loss.  
 224 Evidence for possible dynamical impacts on the vortex is likewise not unequivocal: The vortex  
 225 was among the larger, stronger, and longer-lived in the SH lower stratosphere, but these condi-  
 226 tions were matched or exceeded by those in 2020, 2021, and several previous years in the MERRA-2  
 227 record since 1980; vortex cold anomalies were even less exceptional. Thus, despite large radia-  
 228 tive, dynamical, and composition perturbations in midlatitudes, the observational evidence shows  
 229 that chemical processing within the 2022 Antarctic stratospheric polar vortex was fairly typical,  
 230 and does not show clear evidence of substantial dynamical vortex perturbations. The dispersal  
 231 of HTHH H<sub>2</sub>O following the Antarctic vortex breakup (e.g., Fig. 1) led to unprecedented high  
 232 H<sub>2</sub>O anomalies throughout the SH, which are expected to linger for at least several years (e.g.,  
 233 Millán et al., 2022; Khaykin et al., 2022), raising the expectation of large perturbations to Antarc-  
 234 tic polar vortex chemistry and the ozone hole in 2023 and beyond. HTHH H<sub>2</sub>O has also been trans-  
 235 ported into the Northern Hemisphere (e.g., Schoeberl et al., 2023), but reached the Arctic vor-

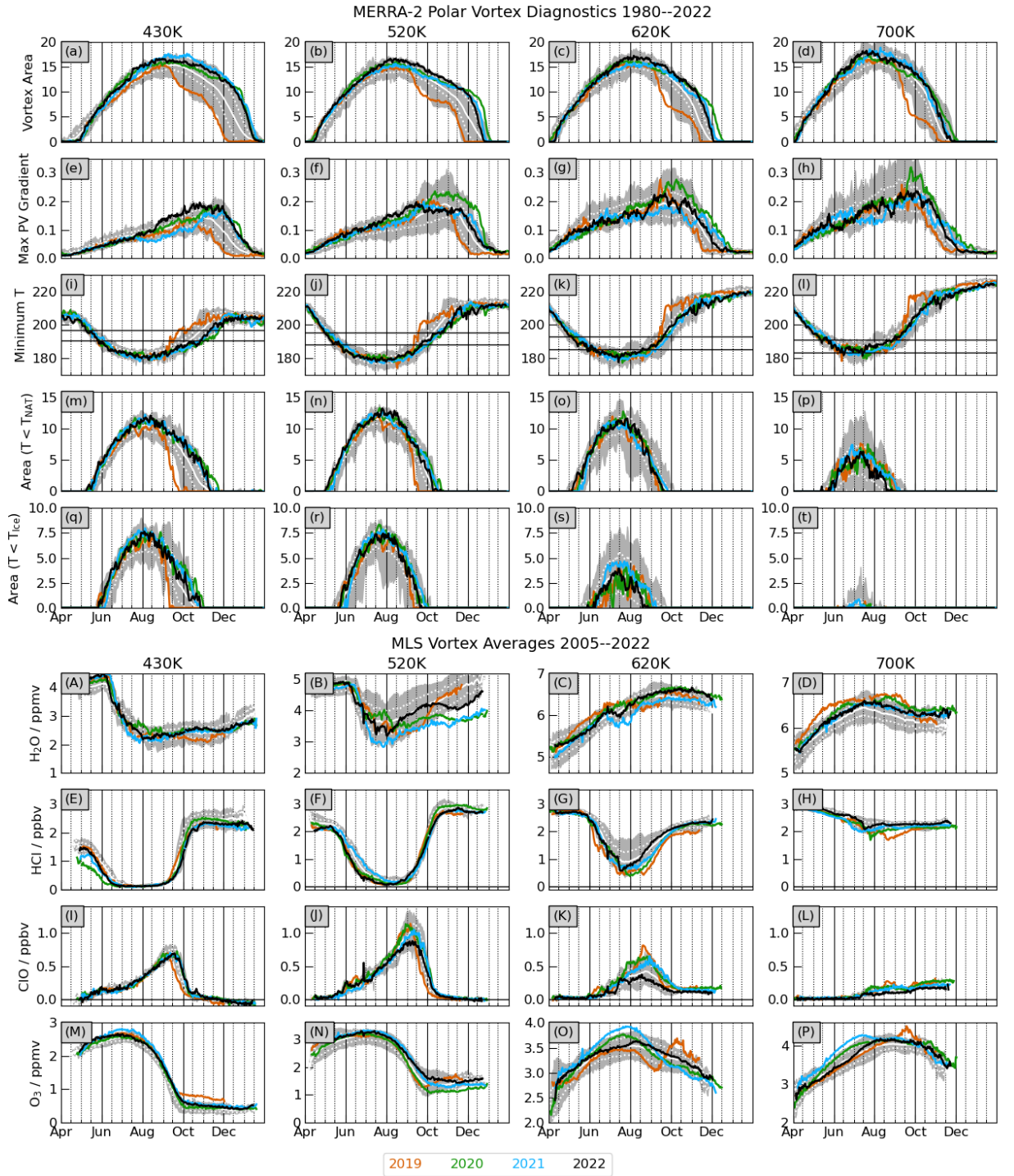


**Figure 4.** (a–t) Time series at four levels in the lower to middle stratosphere of vortex area, maximum PV gradients, high latitude (poleward of  $30^\circ$ ) minimum temperature, and area below NAT and ice PSC thresholds, comparing 2019 (orange), 2020 (green), 2021 (cyan), and 2022 (black) with the range (shading), mean (solid white line), and one standard deviation envelope (dotted white lines) over 1980–2018. (A–P) Vortex-averaged  $\text{H}_2\text{O}$ , HCl, ClO, and  $\text{O}_3$  in same format as for the dynamical fields, with the range over 2005–2018.

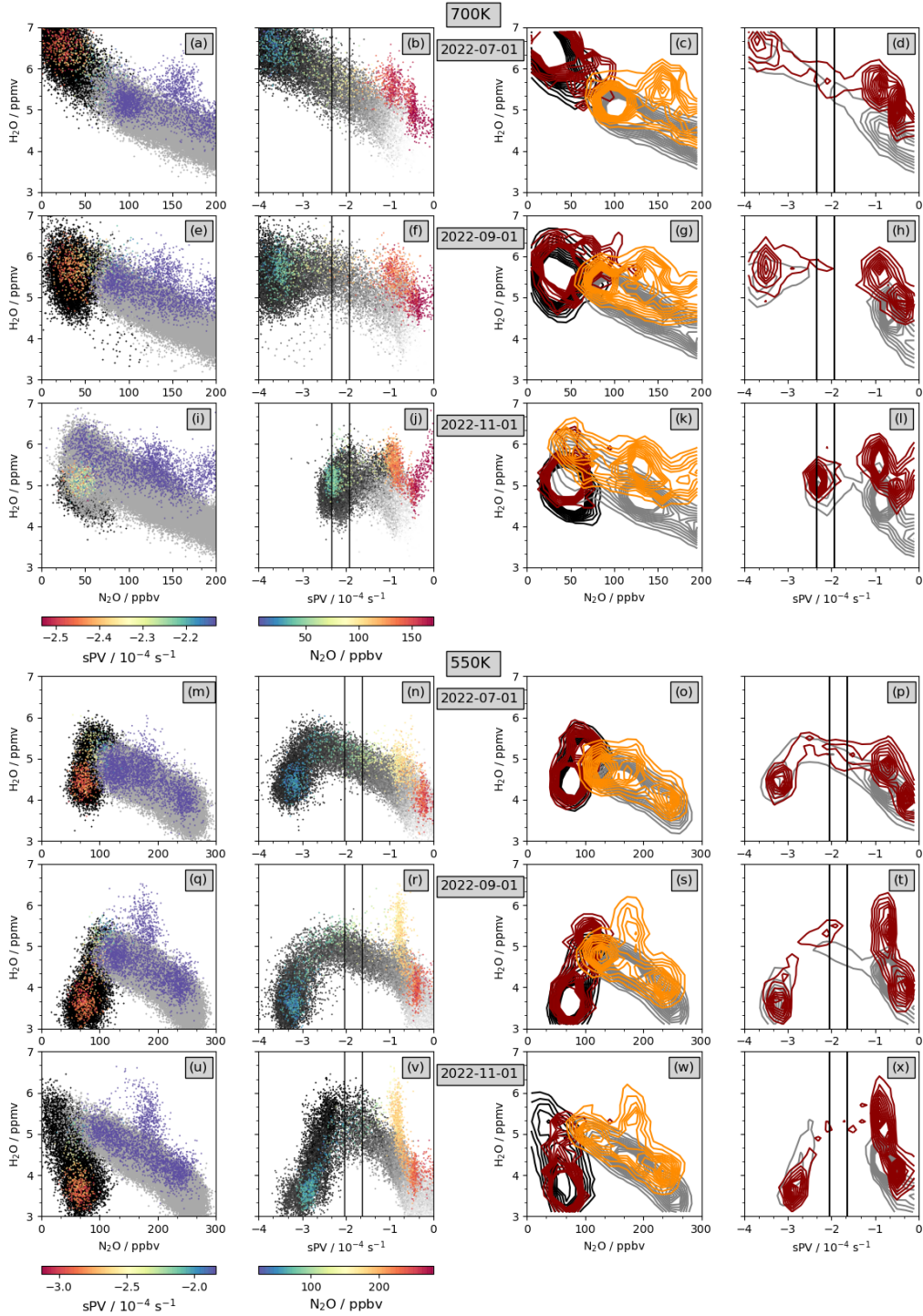


**Figure 5.** Scatter (left two columns) and density (right two columns) plots of MLS H<sub>2</sub>O (y-axis) versus N<sub>2</sub>O (first and third columns) and sPV (second and last columns). Grey and black dots (contours) show values from 2005–2021 in the scatter (density) plots; for those years, black (grey) indicates x-axis values of N<sub>2</sub>O or sPV characteristic of inside (outside) the vortex. For 2022, colored (purple) dots or dark red (orange) contours show sPV values inside (outside) the vortex. 2022 N<sub>2</sub>O (second column) is colored such that blue/blue-green shows typical vortex values. Black vertical lines on the plots versus sPV indicate the vortex edge region.

236 tex edge after the vortex was well-developed and was only dispersed through the NH after a strong  
 237 sudden stratospheric warming starting in mid-February (paper in preparation). Thus large effects  
 238 on Arctic polar vortex chemistry are also expected to manifest starting in the 2023/2024 cool sea-  
 239 son.

## 240 6 Open Research

241 The data used herein are publicly available as follows:

- 242 • MERRA-2: (Global Modeling and Assimilation Office (GMAO), 2015)  
 243 <https://disc.sci.gsfc.nasa.gov/uu/datasets?keywords=%22MERRA-2%22>
- 244 • Aura MLS Level-2 and Level-3 data: (Lambert, Read, & Livesey, 2020; Lambert, Livesey,  
 245 & Read, 2020; Lambert et al., 2021b, 2021a; Schwartz, Pumphrey, et al., 2020; Schwartz,  
 246 Froidevaux, et al., 2020; Schwartz, Pumphrey, et al., 2021; Schwartz, Froidevaux, et al.,  
 247 2021)  
 248 <https://disc.gsfc.nasa.gov/datasets?page=1&keywords=AURA%20MLS>
- 249 • ACE-FTS v4.1/4.2 data: <http://www.ace.uwaterloo.ca> (registration required)
- 250 • ACE-FTS v4.1/4.2 error flags: [https://dataverse.scholarsportal.info/api/access/  
 251 dataset/:persistentId/versions/:latest?persistentId=doi:10.5683/SP2/  
 252 BC4ATC](https://dataverse.scholarsportal.info/api/access/dataset/:persistentId/versions/:latest?persistentId=doi:10.5683/SP2/BC4ATC)
- 253 • MLS & ACE-FTS derived meteorological products: [https://mls.jpl.nasa.gov/eos  
 254 -aura-mls/dmp](https://mls.jpl.nasa.gov/eos-aura-mls/dmp) (registration required).

## 255 Acknowledgments

256 Thanks to the MLS team at JPL for data processing and analysis support, especially Brian Knosp  
 257 for data management, Ryan Fuller for development and production of the MLS L3 products, and  
 258 Lucien Froidevaux and Michael Schwartz for helpful discussions. Thanks to the ACE science  
 259 team for making the ACE-FTS data available, especially Kaley Walker and Patrick Sheese for  
 260 advice on data quality and usage. Thanks to the GMAO for providing the MERRA-2 dataset. G.L. Man-  
 261 ney was supported by the Jet Propulsion Laboratory (JPL) Microwave Limb Sounder team un-  
 262 der JPL subcontract #1521127 to Nwra. Work at the Jet Propulsion Laboratory, California In-  
 263 stitute of Technology, was carried out under a contract with the National Aeronautics and Space  
 264 Administration (80NM0018D0004).

## 265 References

- 266 Baldwin, M. P., Gray, L. J., Dunkerton, T. J., Hamilton, K., Haynes, P. H., J. W., ... Taka-  
 267 hasi, M. (2001). The quasi-biennial oscillation. *Rev. Geophys.*, *39*, 179–229.
- 268 Boone, C., Bernath, P., Cok, D., Jones, S., & Steffen, J. (2020). Version 4 retrievals for the  
 269 atmospheric chemistry experiment Fourier transform spectrometer (ACE-FTS) and  
 270 imagers. *Journal of Quantitative Spectroscopy and Radiative Transfer*, *247*, 106939.  
 271 Retrieved from [https://www.sciencedirect.com/science/article/pii/  
 272 S0022407319305916](https://www.sciencedirect.com/science/article/pii/S0022407319305916) doi: <https://doi.org/10.1016/j.jqsrt.2020.106939>
- 273 Butchart, N., & Remsberg, E. E. (1986). The area of the stratospheric polar vortex as a diag-  
 274 nostic for tracer transport on an isentropic surface. *J. Atmos. Sci.*, *43*, 1319–1339.
- 275 Coy, L., Newman, P. A., Wargan, K., Partyka, G., Strahan, S. E., & Pawson,  
 276 S. (2022). Stratospheric Circulation Changes Associated With the  
 277 Hunga Tonga-Hunga Ha’apai Eruption. *Geophysical Research Let-  
 278 ters*, *49*(22), e2022GL100982. Retrieved 2022-11-27, from [https://  
 279 onlinelibrary.wiley.com/doi/abs/10.1029/2022GL100982](https://onlinelibrary.wiley.com/doi/abs/10.1029/2022GL100982) (eprint:  
 280 <https://onlinelibrary.wiley.com/doi/pdf/10.1029/2022GL100982>) doi: 10.1029/  
 281 2022GL100982
- 282 Diallo, M., Konopka, P., Santee, M. L., Müller, R., Tao, M., Walker, K. A., ... Ploeger,

- 283 F. (2019). Structural changes in the shallow and transition branch of the Brewer–  
 284 Dobson circulation induced by El Niño. *Atmos. Chem. Phys.*, *19*(1), 425–446. Re-  
 285 trieved from <https://acp.copernicus.org/articles/19/425/2019/> doi:  
 286 10.5194/acp-19-425-2019
- 287 Gelaro, R., McCarty, W., Suárez, M. J., Todling, R., Molod, A., Takacs, L., . . . Zhao, B.  
 288 (2017). The Modern-Era Retrospective Analysis for Research and Applications,  
 289 Version-2 (MERRA-2). *J. Clim.*, *30*, 5419–5454. doi: doi:10.1175/JCLI-D-16-0758.1
- 290 Global Modeling and Assimilation Office (GMAO). (2015). *MERRA-2 inst3\_3d\_asm\_nv:*  
 291 *3d, 3-hourly, instantaneous, model-level, assimilation, assimilated meteorolog-*  
 292 *ical fields v5.12.4, Greenbelt, MD, USA, Goddard Earth Sciences Data and In-*  
 293 *formation Services Center (GES DISC), accessed 1 June 2022* [dataset]. doi:  
 294 10.5067/WWQSQXQ8IVFW8
- 295 Khaykin, S., Podglajen, A., Ploeger, F., Grooß, J.-U., Tence, F., Bekki, S., . . . Ravetta, F.  
 296 (2022, December). Global perturbation of stratospheric water and aerosol burden by  
 297 Hunga eruption. *Communications Earth & Environment*, *3*(1), 316. Retrieved from  
 298 <https://doi.org/10.1038/s43247-022-00652-x>
- 299 Lambert, A., Livesey, N., & Read, W. (2020). *MLS/Aura level 2 nitrous oxide (N2O)*  
 300 *mixing ratio V005, Greenbelt, MD, USA, Goddard Earth Sciences Data and In-*  
 301 *formation Services Center (GES DISC), accessed: [26 June 2022]* [dataset]. doi:  
 302 <https://doi.org/10.5067/Aura/MLS/DATA2515>
- 303 Lambert, A., Livesey, N., Read, W., & Fuller, R. (2021a). *MLS/Aura level 3 daily*  
 304 *binned nitrous oxide (N2O) mixing ratio on zonal and similar grids V005, Green-*  
 305 *belt, MD, USA, Goddard Earth Sciences Data and Information Services Cen-*  
 306 *ter (GES DISC), accessed: [26 June 2022]* [dataset]. Retrieved from [https://](https://disc.gsfc.nasa.gov/datasets/ML3DZN20_005/summary?keywords=mls)  
 307 [disc.gsfc.nasa.gov/datasets/ML3DZN20\\_005/summary?keywords=mls](https://disc.gsfc.nasa.gov/datasets/ML3DZN20_005/summary?keywords=mls) doi:  
 308 <https://doi.org/10.5067/Aura/MLS/DATA/3116>
- 309 Lambert, A., Livesey, N., Read, W., & Fuller, R. (2021b). *MLS/Aura level 3 daily*  
 310 *binned water vapor (H2O) mixing ratio on zonal and similar grids V005, Green-*  
 311 *belt, MD, USA, Goddard Earth Sciences Data and Information Services Cen-*  
 312 *ter (GES DISC), accessed: [26 June 2022]* [dataset]. Retrieved from [https://](https://disc.gsfc.nasa.gov/datasets/ML3DZH20_005/summary?keywords=mls)  
 313 [disc.gsfc.nasa.gov/datasets/ML3DZH20\\_005/summary?keywords=mls](https://disc.gsfc.nasa.gov/datasets/ML3DZH20_005/summary?keywords=mls) doi:  
 314 <https://doi.org/10.5067/Aura/MLS/DATA/3109>
- 315 Lambert, A., Read, W., & Livesey, N. (2020). *MLS/Aura Level 2 water vapor (H2O)*  
 316 *mixing ratio V005, Greenbelt, MD, USA, Goddard Earth Sciences Data and In-*  
 317 *formation Services Center (GES DISC), accessed: [26 June 2022]* [dataset]. doi:  
 318 <https://doi.org/10.5067/Aura/MLS/DATA2508>
- 319 Lee, J. N., Wu, D. L., Manney, G. L., Schwartz, M. J., Lambert, A., Livesey, N. J., . . . Read,  
 320 W. G. (2011). Aura Microwave Limb Sounder observations of the polar middle  
 321 atmosphere: Dynamics and transport of CO and H<sub>2</sub>O. *J. Geophys. Res.*, *116*. doi:  
 322 10.1029/2010JD014608
- 323 Legras, B., Duchamp, C., Sellitto, P., Podglajen, A., Carboni, E., Siddans, R., . . . Ploeger,  
 324 F. (2022, November). The evolution and dynamics of the Hunga Tonga–Hunga  
 325 Ha’apai sulfate aerosol plume in the stratosphere. *Atmospheric Chemistry*  
 326 *and Physics*, *22*(22), 14957–14970. Retrieved 2022-11-23, from [https://](https://acp.copernicus.org/articles/22/14957/2022/)  
 327 [acp.copernicus.org/articles/22/14957/2022/](https://acp.copernicus.org/articles/22/14957/2022/) (Publisher: Copernicus  
 328 GmbH) doi: 10.5194/acp-22-14957-2022
- 329 Livesey, N. J., Read, W. G., Wagner, P. A., Froidevaux, L., Lambert, A., Manney, G. L., . . .  
 330 Lay, R. R. (2020). *EOS MLS version 5.0x level 2 and 3 data quality and description*  
 331 *document* (Tech. Rep.). JPL. (Available from <http://mls.jpl.nasa.gov/>)
- 332 Millán, L., et al. (2022). The Hunga Tonga-Hunga Ha’apai hydration of the strato-  
 333 sphere. *Geophys. Res. Lett.*, *49*(13), e2022GL099381. Retrieved from [https://](https://agupubs.onlinelibrary.wiley.com/doi/abs/10.1029/2022GL099381)  
 334 [agupubs.onlinelibrary.wiley.com/doi/abs/10.1029/2022GL099381](https://agupubs.onlinelibrary.wiley.com/doi/abs/10.1029/2022GL099381)  
 335 (e2022GL099381 2022GL099381) doi: <https://doi.org/10.1029/2022GL099381>
- 336 Randel, W. J., Moyer, E., Park, M., Jensen, E., Bernath, P., Walker, K., & Boone, C.  
 337 (2012). Global variations of HDO and HDO/H<sub>2</sub>O ratios in the upper troposphere

- 338 and lower stratosphere derived from ACE-FTS satellite measurements. *Journal of Geophysical Research: Atmospheres*, 117(D6). Retrieved from <https://agupubs.onlinelibrary.wiley.com/doi/abs/10.1029/2011JD016632> doi: <https://doi.org/10.1029/2011JD016632>
- 339  
340  
341
- 342 Ray, E. A., Moore, F. L., Elkins, J. W., Hurst, D. F., Romashkin, P. A., Dutton, G. S., &  
343 Fahey, D. W. (2002). Descent and mixing in the 1999-2000 northern polar vortex  
344 inferred from in situ tracer measurements. *J. Geophys. Res.*, 107, 8285. doi:  
345 10.1029/2001JD000961
- 346 Santee, M. L., Lambert, A., Manney, G. L., Livesey, N. J., Froidevaux, L., Neu, J. L., ...  
347 Ward, B. M. (2022). Prolonged and pervasive perturbations in the composition of  
348 the Southern Hemisphere midlatitude lower stratosphere from the Australian New  
349 Year's fires. *Geophysical Research Letters*, 49(4), e2021GL096270. Retrieved  
350 from [https://agupubs.onlinelibrary.wiley.com/doi/abs/10.1029/](https://agupubs.onlinelibrary.wiley.com/doi/abs/10.1029/2021GL096270)  
351 [2021GL096270](https://doi.org/10.1029/2021GL096270) (e2021GL096270 2021GL096270) doi: [https://doi.org/10.1029/](https://doi.org/10.1029/2021GL096270)  
352 [2021GL096270](https://doi.org/10.1029/2021GL096270)
- 353 Santee, M. L., MacKenzie, I. A., Manney, G. L., Chipperfield, M. P., Bernath, P. F., Walker,  
354 K. A., ... Waters, J. W. (2008). A study of stratospheric chlorine partitioning  
355 based on new satellite measurements and modeling. *J. Geophys. Res.*, 113. doi:  
356 10.1029/2007JD009057
- 357 Schoeberl, M. R., Wang, Y., Ueyama, R., Taha, G., Jensen, E., & Yu, W. (2022). Anal-  
358 ysis and impact of the Hunga Tonga-Hunga Ha'apai stratospheric water vapor  
359 plume. *Geophys. Res. Lett.*, 49(20), e2022GL100248. Retrieved from <https://agupubs.onlinelibrary.wiley.com/doi/abs/10.1029/2022GL100248>  
360 (e2022GL100248 2022GL100248) doi: <https://doi.org/10.1029/2022GL100248>
- 361 Schoeberl, M. R., Wang, Y., Ueyama, R., Taha, G., & Yu, W. (2023). The cross  
362 equatorial transport of the Hunga Tonga-Hunga Ha'apai eruption plume. *Geo-*  
363 *physical Research Letters*, 50(4), e2022GL102443. Retrieved from <https://agupubs.onlinelibrary.wiley.com/doi/abs/10.1029/2022GL102443>  
364 (e2022GL102443 2022GL102443) doi: <https://doi.org/10.1029/2022GL102443>
- 365  
366
- 367 Schwartz, M., Froidevaux, L., Livesey, N., & Read, W. (2020). *MLS/Aura level 2 ozone*  
368 *(O3) mixing ratio V005, Greenbelt, MD, USA, Goddard Earth Sciences Data and*  
369 *Information Services Center (GES DISC), accessed: [26 June 2022]* [dataset]. doi:  
370 <https://doi.org/10.5067/Aura/MLS/DATA2506>
- 371 Schwartz, M., Froidevaux, L., Livesey, N., Read, W., & Fuller, R. (2021). *MLS/Aura*  
372 *level 3 daily binned ozone (O3) mixing ratio on zonal and similar grids V005,*  
373 *Greenbelt, MD, USA, Goddard Earth Sciences Data and Information Services Cen-*  
374 *ter (GES DISC), accessed: [26 June 2022]* [dataset]. Retrieved from [https://disc.gsfc.nasa.gov/datasets/ML3DZ03\\_005/summary?keywords=mls](https://disc.gsfc.nasa.gov/datasets/ML3DZ03_005/summary?keywords=mls) doi:  
375 <https://doi.org/10.5067/Aura/MLS/DATA/3105>
- 376  
377
- 378 Schwartz, M., Pumphrey, H., Livesey, N., & Read, W. (2020). *MLS/Aura level 2 car-*  
379 *bon monoxide (CO) mixing ratio V005, Greenbelt, MD, USA, Goddard Earth Sci-*  
380 *ences Data and Information Services Center (GES DISC), accessed: [26 June 2022]*  
381 [dataset]. doi: <https://doi.org/10.5067/Aura/MLS/DATA2506>
- 382 Schwartz, M., Pumphrey, H., Livesey, N., Read, W., & Fuller, R. (2021). *MLS/Aura level*  
383 *3 daily binned carbon monoxide (CO) mixing ratio on zonal and similar grids V005,*  
384 *Greenbelt, MD, USA, Goddard Earth Sciences Data and Information Services Cen-*  
385 *ter (GES DISC), accessed: [26 June 2022]* [dataset]. Retrieved from [https://disc.gsfc.nasa.gov/datasets/ML3DZC0\\_005/summary?keywords=mls](https://disc.gsfc.nasa.gov/datasets/ML3DZC0_005/summary?keywords=mls) doi:  
386 <https://doi.org/10.5067/Aura/MLS/DATA/3105>
- 387 Sellitto, P., Podglajen, A., Belhadji, R., Boichu, M., Carboni, E., Cuesta, J., ... Legras, B.  
388 (2022, November). The unexpected radiative impact of the Hunga Tonga eruption of  
389 15th January 2022. *Communications Earth & Environment*, 3(1), 1–10. Retrieved  
390 2022-11-27, from <https://www.nature.com/articles/s43247-022-00618-z>  
391 (Number: 1 Publisher: Nature Publishing Group) doi: 10.1038/s43247-022-00618-z
- 392 Sheese, P. E., Walker, K. A., Boone, C. D., Bourassa, A. E., Degenstein, D. A., Froide-

- 393 vaux, L., ... Zou, J. (2022). Assessment of the quality of ACE-FTS stratospheric  
394 ozone data. *Atmospheric Measurement Techniques*, 15(5), 1233–1249. Re-  
395 trieved from <https://amt.copernicus.org/articles/15/1233/2022/> doi:  
396 10.5194/amt-15-1233-2022
- 397 Taha, G., Loughman, R., Colarco, P. R., Zhu, T., Thomason, L. W., & Jaross, G.  
398 (2022). Tracking the 2022 Hunga Tonga-Hunga Ha’apai Aerosol Cloud in the  
399 Upper and Middle Stratosphere Using Space-Based Observations. *Geophys-*  
400 *ical Research Letters*, 49(19), e2022GL100091. Retrieved 2022-10-13, from  
401 <https://onlinelibrary.wiley.com/doi/abs/10.1029/2022GL100091>  
402 (eprint: <https://onlinelibrary.wiley.com/doi/pdf/10.1029/2022GL100091>) doi:  
403 10.1029/2022GL100091
- 404 Vömel, H., Evan, S., & Tully, M. (2022, September). Water vapor injection into the strato-  
405 sphere by Hunga Tonga-Hunga Ha’apai. *Science*, 377(6613), 1444–1447. Retrieved  
406 2022-11-27, from <https://www.science.org/doi/10.1126/science.abq2299>  
407 (Publisher: American Association for the Advancement of Science) doi: 10.1126/  
408 science.abq2299
- 409 Wargan, K., Weir, B., Manney, G. L., Cohn, S. E., & Livesey, N. J. (2020). The anoma-  
410 lous 2019 Antarctic ozone hole in the GEOS constituent data assimilation system  
411 with MLS observations. *Journal of Geophysical Research: Atmospheres*, 125(18),  
412 e2020JD033335. Retrieved from [https://agupubs.onlinelibrary.wiley.com/](https://agupubs.onlinelibrary.wiley.com/doi/abs/10.1029/2020JD033335)  
413 [doi/abs/10.1029/2020JD033335](https://doi.org/10.1029/2020JD033335) (e2020JD033335 2020JD033335) doi:  
414 <https://doi.org/10.1029/2020JD033335>
- 415 WMO. (2023). *Scientific assessment of ozone depletion: 2022*. Geneva, Switzerland: Global  
416 Ozone Res. and Monit. Proj. Rep. 55.
- 417 Zhu, Y., Bardeen, C. G., Tilmes, S., Mills, M. J., Wang, X., Harvey, V. L., ... Toon, O. B.  
418 (2022, October). Perturbations in stratospheric aerosol evolution due to the water-rich  
419 plume of the 2022 Hunga-Tonga eruption. *Communications Earth & Environment*,  
420 3(1), 1–7. Retrieved 2022-11-27, from [https://www.nature.com/articles/](https://www.nature.com/articles/s43247-022-00580-w)  
421 [s43247-022-00580-w](https://www.nature.com/articles/s43247-022-00580-w) (Number: 1 Publisher: Nature Publishing Group) doi:  
422 10.1038/s43247-022-00580-w